

Orthographic Imaging of Free-Flowing Aerosol Particles

JESSE C. LANING¹, MATTHEW J. BERG^{1,*}

¹Department of Physics, Kansas State University, 1228 N. 17th St., Manhattan, KS 66506-2601, USA

*Corresponding author: matt.berg@phys.ksu.edu

Received XX Month XXXX; revised XX Month, XXXX; accepted XX Month XXXX; posted XX Month XXXX (Doc. ID XXXXX); published XX Month XXXX

A method to obtain contact-free images of aerosol particles with digital holography from three orthogonal directions is described. The approach uses three diode lasers of different wavelengths to simultaneously illuminate flowing particles and form holograms on three sensors. Images of the particles are then reconstructed from the holograms and used to infer the three-dimensional structure of the particles. The apparatus employs inexpensive components and does not require lenses to achieve the imaging, giving it a large sensing volume and simple design. Test cases are presented with spherical glass particles and nonspherical pollen particles.

<http://dx.doi.org/10.1364/OL.99.099999>

The ability to image particles micrometers in size in a three-dimensional (3D) manner is useful for many applications in medicine, science, and industry [1]. For example, particle-type differentiation, and even identification in some cases, can be aided by the knowledge of a particle's 3D form. Such information is also useful to estimate particle volume. Methods are available in conventional imaging to resolve or reconstruct the 3D form of particles of this size, such as confocal microscopy and X-ray or electron tomographic microscopy [2,3]. However, these methods require collection or trapping of the particles, and as such, they are not useful in cases where particles must be observed *in situ*, although there are notable exceptions in [4,5]. Aerosol particles are one example where contact-free imaging is preferred to avoid shape-related particle collection artifacts, or is required, as is the case for ice or liquid-drop particles. This Letter presents an experiment where multiple two-dimensional (2D) images of individual free-flowing aerosol particles are obtained using in-line digital holography (DH) without the need to collect or trap the particles. The images are then combined to infer the 3D form of the particles.

In previous work employing DH, a particle or a collection of particles is illuminated by a laser beam and the interference pattern, i.e., hologram, produced by the particle's forward scattered light and the beam is recorded by a CCD sensor [6]. Applying Fresnel-

Kirchhoff (FK) scalar diffraction theory to the hologram then yields a silhouette-like 2D image of the particle from the perspective of the beam direction [7]. By pulsing the laser, free-flowing particles can be imaged, and a number of useful quantiles can be derived in addition to an image such as the particle's scattering pattern and extinction cross section [6,8]. Examples of such 2D imaging include [9] where laboratory generated aerosols are investigated, and the HOLODEC instruments in [10] where cloud aerosol particles are observed from aircraft in the field. Work that achieves 3D imaging via DH or related methods is found in [11-13]. In many of these examples the true 3D form of the particles is difficult to discern from the 2D images obtained, e.g., see [13]. The goal here is to establish if DH can be implemented in such a way as to provide an improved realization of a particle's 3D by viewing the particles from different perspectives.

The apparatus shown in Fig. 1 achieves this goal. A hollow mounting cube with 25.4 mm diameter (\emptyset) threaded holes through each face is shown in the top view in Fig. 1(a). In three of these holes that share a common cube-corner are 25.4 mm \emptyset lens tubes (although no lenses are used). Mounted to the ends of each tube is a diode laser (DL), each emitting at a different wavelength: $\lambda_r = 660$ nm or "red" for short, $\lambda_g = 520$ nm, or "green," and $\lambda_b = 450$ nm, "blue." The beam path for the blue and green DLs can be seen in the side view in Fig. 1(b). Opposite each DL at the far cube-face is a bandpass filter, corresponding to the DL's wavelength, followed by a board-level monochrome CMOS sensor. A small hole approximately 1 mm \emptyset is drilled through the cube along its main diagonal from one apex to another as shown in Fig. 1(a) and 1(b). The hole allows an aerosol stream to be passed from top to bottom through the central region of the cube where the particles are simultaneously illuminated by the three orthogonal DLs and the resulting holograms are recorded.

Board-level sensors are used to allow the hologram recording to be as close to the aerosol stream as practical, which improves the eventual image resolution and gives the apparatus a small form-factor of approximately 10×10×10 cm. These sensors (FLIR, BFS-U3-50S5-BD) have an array size of 2448×2048 pixels, with a pixel size of 3.45× 3.45 μm , and a global shutter readout. Clear hologram fringes are recorded by pulsing the DLs simultaneously to emit for a 200 ns period after the electronic-shutter activation, having the effect of freezing-out the particle motion.

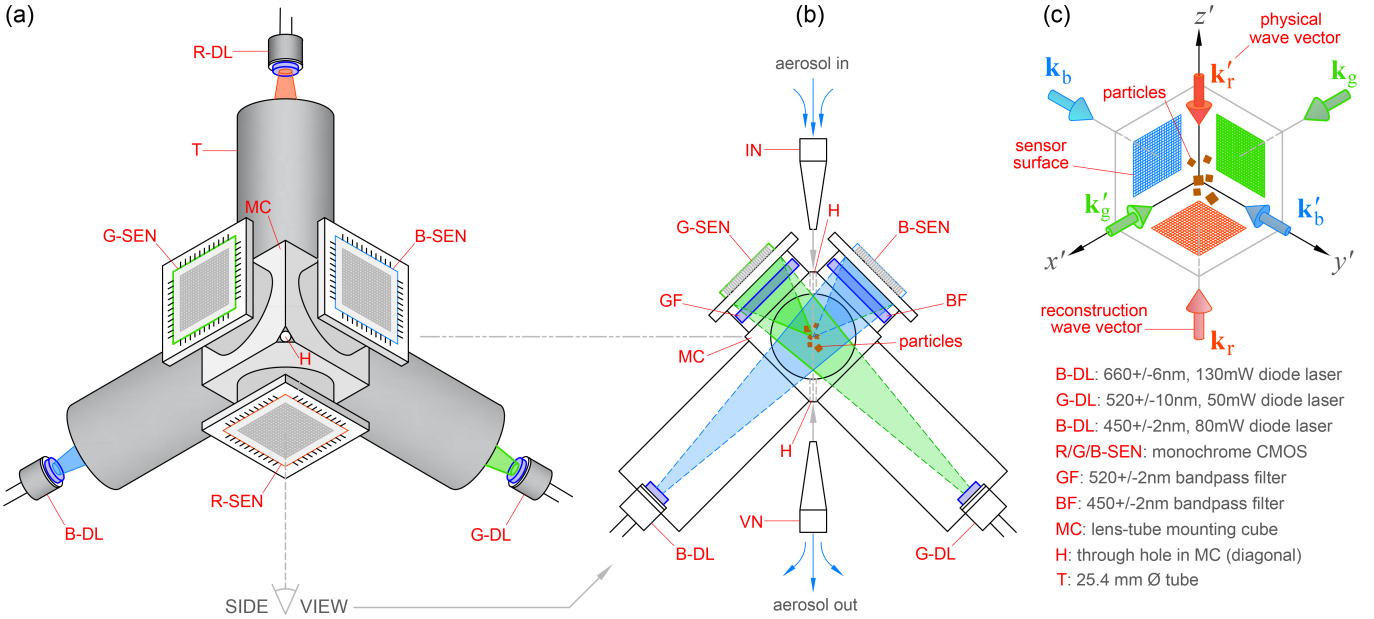


Fig. 1. Sketch of the orthographic imaging apparatus and coordinate systems. In (a), is a top view showing the major components. An aerosol stream is delivered to the sensing volume via a nozzle [shown in (b) as (IN)] through a hole (H) at the top apex of a hollow aluminum “mounting” cube (MC). The particles are removed under negative pressure applied to a corresponding hole and nozzle (VN) at the bottom apex. Lens tubes (T) are connected to each face of the cube as shown. A red, green, or blue diode laser (DL) is mounted at the ends of the three long tubes to illuminate the aerosol flow and three CMOS sensors (SEN) at the opposite cube faces. Guarding each sensor is a bandpass filter matched to the DL opposite the sensor. Two of these filters (GF) and (BF) are visible in (b) where a side view of the apparatus is shown from the perspective indicated in (a). Sketch (b) also shows the unscattered and scattered light from the particles that forms the holograms. Finally, (c) shows the three sensor surfaces defining the SCS, the particles, and the physical and reconstruction wave vectors, \mathbf{k}'_n and \mathbf{k}_n .

The purpose of the bandpass filters is to ensure that only light from the DL across the cube from a sensor reaches that sensor’s surface. In other words, the filters prevent optical “cross talk” between the sensors. This is preferable to pulsing the DLs sequentially because the likelihood that the particles would change orientation between each pulse.

Because each hologram is formed by illuminating the same group of particles from a different orthogonal direction, the 3D form of a given particle can be inferred from the 2D images, or “views,” that are reconstructed from each hologram. As will be seen below, this inference is incomplete, yet is vastly better than what is typically achieved from a single viewing direction in DH.

Particle-image reconstruction begins with a background measurement, which is simply an exposure of the sensors to the DL pulses when no particles are present. This background is then subtracted from the same measurement when the particles are present. The result is a contrast hologram I^{con} of which there are three corresponding to the orthogonal views: I_r^{con} , I_g^{con} , and I_b^{con} . Both the particle-free and particle-present exposures are obtained with DL pulses of the same duration, i.e., 200 ns. Each contrast hologram is then used in the FK integral [7,14],

$$K_n(\eta, \xi) = \alpha_n \iint_S I_n^{\text{con}}(\eta', \xi') g(\eta, \xi, \eta', \xi') d\eta' d\xi', \quad (1)$$

which is simplified here by use of the Fresnel approximation in that

$$g(\eta, \xi, \eta', \xi') = \exp \left\{ \frac{i k_n}{2 d_n} [(\eta - \eta')^2 + (\xi - \xi')^2] \right\}. \quad (2)$$

In Eqs. (1)-(2), $n = \{r, g, b\}$ to denote the three DL wavelengths λ_n , $\alpha_n = id_n/\lambda_n$, $k_n = 2\pi/\lambda_n$, S is the surface of the n^{th} sensor where contrast hologram I_n^{con} is measured, and d_n is the particle-sensor separation, or “focus distance,” for the n^{th} view. Evaluating $|K_n|^2$ gives the 2D particle image for n^{th} view by iteratively adjusting the value of d_n until the image develops a clear focus [13].

The 2D views must then be arranged in 3D space in a way that best conveys a particle’s 3D form. To explain how this is done, refer to Fig. 1(c) where the sensor surfaces are shown in the sensor coordinate system (x', y', z') , abbreviated as SCS, along with the corresponding DL wave vectors, \mathbf{k}'_n . Equation (1) is evaluated for each I_n^{con} using auxiliary coordinates (η', ξ') and a reconstruction wave vector $\mathbf{k}_n = -\mathbf{k}'_n$, where the coordinate associated with \mathbf{k}_n is perpendicular to the (η', ξ') plane. The particle images then reside in the particle coordinate system (x, y, z) , or PCS. For example, consider the red viewing direction, $n = r$. Here, the auxiliary coordinates would be $\eta' = x'$ and $\xi' = y'$ because I_r^{con} resides in the (x', y') plane in the SCS. If the physical wave vector $\mathbf{k}'_r = k_r \hat{\mathbf{z}}$ were used to evaluate Eq. (1), the particle image would be generated in the $(\eta = x, \xi = y)$ plane in the PCS at a distance d_r along the negative z -axis, i.e., one obtains the virtual particle-image. Using the reconstruction wave vector \mathbf{k}_r generates the image along the positive z -axis where the particles actually reside. In other words, the reconstruction uses the backpropagation of the DL light. Alternatively, \mathbf{k}'_r can be used provided $d_r \rightarrow -d_r$, which can be seen to have the same effect from Eq. (2).

Once reconstructed, the three images are positioned in the PCS such that each corresponds to the geometric projection of the particles along a given viewing direction. Figure (2) shows an example. Here, the particles are a powder of glass microspheres with mean radii of $R_s = 25 \mu\text{m}$ that are aerosolized and passed to the injection nozzle (IN) in Fig. (1). A large number of aerosol particles pass through the beams and are removed by another nozzle (VN) by a weak vacuum line. Simultaneously pulsing the DLs results in the contrast holograms shown in Fig. 2(a), which are color coded to match the DL wavelengths. Close inspection reveals that each exhibit an intricate fringe pattern with features associated with individual particles. Application of Eq. (1) to these holograms as described above yield the orthographic images shown in Fig. 2(b) in the PCS where the silhouettes are color coded to match the DL light as in Fig. 2(a). Note that the holograms in Fig. 2(a) are slightly cropped to a square size of 2048×2048 pixels rather than the full-sensor size of 2448×2048 pixels.

By surveying the relative position of all silhouettes in the three views, it is usually possible to identify a “fiducial” silhouette in each that corresponds to the same, single particle. A circle is then drawn enclosing this silhouette in each view, defining three radii R_r , R_g , and R_b . From each radius, a scale factor α_n is determined such that the radii equal the known particle size, i.e., $\alpha_r R_r = \alpha_g R_g = \alpha_b R_b = R_s$. The centers of these circles also allow the views to be correctly positioned in the PCS by translating each image in its own plane such that back projection of the circles corresponds to the center of a single spherical particle. Figure 2(b) shows dashed lines denoting this back-projection to two spheres. Note that the 3D sphere shapes here are artificially drawn while the silhouettes are real images.

Once the scale factors α_n are identified, other particle types can be investigated with the PCS axes scaled to micrometers. An example is presented in Fig. 3 where a powder of dried, dead ragweed pollen grains is used as the particle source. These are spherical-like particles on the order of $20 - 30 \mu\text{m} \varnothing$ with an echinate surface that promotes clustering of individual grains. The contrast holograms are presented in Fig. 3(a) and the resulting views are shown in Fig. 3(b). As before, a circle enclosing the silhouette of a single cluster is drawn in each view and the views are then positioned in 3D space via the circles’ centers in the PCS. Once positioned, $22 \mu\text{m} \varnothing$ spheres are placed in the PCS such that their projections onto the image planes approximately agree with the silhouettes. The sphere size is determined from the blue and green views where outlines of individual grains in most of the cluster can be discerned. Figure 3(b) shows the result of this process where the blue and green-views are included as insets. Close inspection reveals a small degree of misalignment between the spheres and projections, which is more an effect of parallax than misplacement of the spheres. Small-scale features of the cluster are not captured by this process such as the surface roughness of the individual grains and void spaces between grains. This is due to the limited image-resolution of the apparatus, which is estimated as $10 \mu\text{m}$ from the features that appear clear in Fig. 3(b). One can also see a lone grain silhouette in the green view in Fig. 3(b) indicated by (*) that is not seen in the other views, and thus, is not represented by a sphere.

The utility of this imaging approach can be appreciated from Fig. 3(b) in that if one were to only have a single view, it would be unlikely to generate a reasonable 3D rendering of the full particle-cluster. Consider the red view in Fig. 3(b) as an example. While this view gives a very approximate sense for the overall size of the

particle, it does not clearly reveal that the particle is a cluster of spherical grains like the other views do. Indeed, from the red view alone, one may not realize the comparatively long extent of the cluster along the z -axis. Such capability could enable an improved estimation for the volume of aerosol particles. This would be useful in meteorological contexts where the volume fractions of water and ice particles in clouds strongly affects cloud-radiation interactions, whether that be radar or sunlight [10].

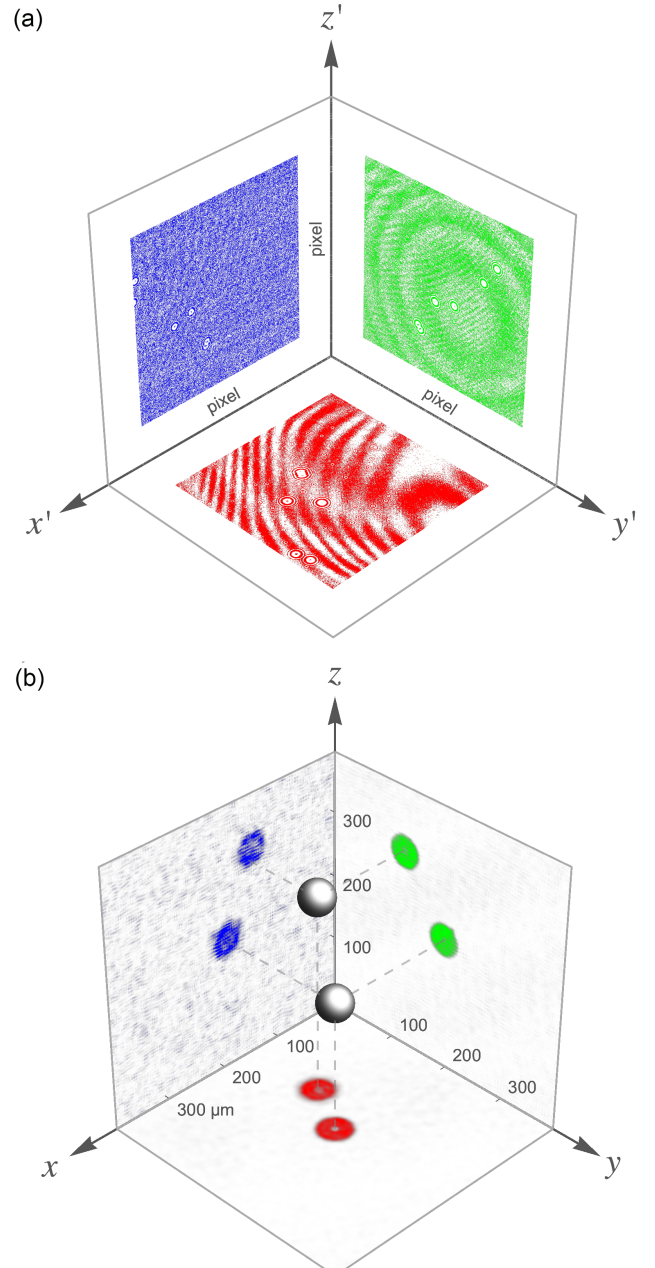


Fig. 2. Orthographic imaging of free-flowing $50 \mu\text{m} \varnothing$ spherical aerosol particles. In (a), the contrast holograms I_r^{con} , I_g^{con} , and I_b^{con} are shown color-coded to denote the DL wavelength. Evaluating Eq. (1) as described in the text generates the 2D particle silhouettes for each viewing direction, shown in (b). The holograms and silhouettes are color-coded to match the DL light. The dashed lines show how the

center points of the silhouettes are back-projected into 3D space to identify the location of each particle, where a sphere is then drawn.

Another useful aspect of this method is the absence of lenses, which gives the apparatus a much larger sensing volume than what is typically available in conventional microscopy. In principle, any particle that occupies the overlap volume of the three DL beams, which is approximately 1 cm^3 , will contribute to the holograms and can be imaged. Of course, the particles must be larger than the image-resolution limit of $10 \mu\text{m}$ to do so.

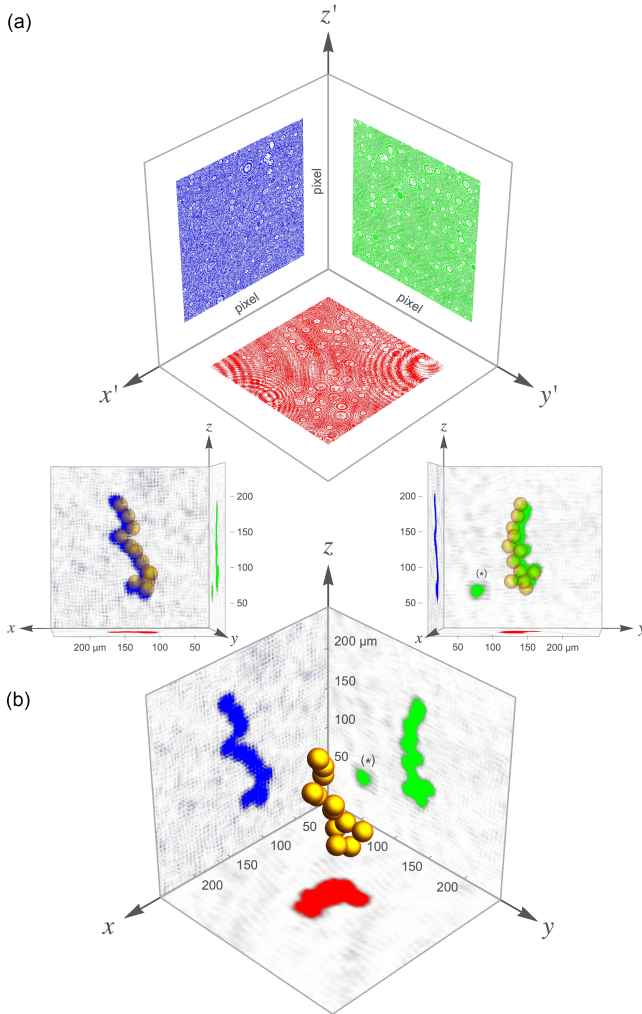


Fig. 3. Orthographic imaging of a ragweed pollen aerosol. In analogy to Fig. 2, (a) shows the contrast holograms and (b) shows the particle silhouettes generated from those holograms for a single particle-cluster. Following alignment of the 2D views via inscribing circles as described in the text, spheres of equal size are placed in 3D space such that their projections onto each of the image planes best agree with the structure seen in each silhouette. To provide more detail, (b) also shows different perspectives of the blue and green views to highlight the correspondence between the silhouettes and the placement of the spheres. The isolated pollen grain labeled (*) is not associated with a sphere because it is visible only in the green view.

The next step for this work is to test more formal techniques, such as weighted back-projection, to better render the 3D form of the

particles [3]. While this is an ill-posed problem with only three views, it should be possible to achieve better reconstructions than the simple sphere or sphere-clusters used here.

Funding. National Science Foundation (NSF) CAREER program (1665456).

Acknowledgment. The authors are grateful for helpful discussions with Stephen Holler, Sungsoo S. Kim, Gorden Videen, electronics design assistance from the KSU Electronics Design Laboratory, and Andrew Thurlow for machining services.

References

1. P. Kulkarni, K. Willeke (eds.), *Aerosol Measurement: Principles, Techniques, and Applications* (Wiley, New Jersey, 2011), p. 752.
2. F. Joachim (ed.) *Electron Tomography: Methods for Three-Dimensional Visualization of Structures in the Cell*, 2nd ed., (Springer, New York, 2006).
3. A. J. Koster, U. Ziese, A. J. Verkleij, A. H. Janssen, K. P. de Jong, *J. Chem. Phys. B* **104**, 9368-9370 (2000).
4. Y.-L. Pan, C. Wang, S. C. Hill, M. Coleman, L. A. Beresnev, J. L. Santarpia, *Appl. Phys. Lett.* **104**, 113507 (2014).
5. N. D. Lho, et al., *Nature* **486**, 513 (2012).
6. M. J. Berg, Y. W. Heinson, O. Kemppinen, S. Holler, *Sci. Rep.* **7**:9400 (2017).
7. T. Kreis, *Handbook of Holographic Interferometry: Optical and Digital Methods* (Wiley, 2005).
8. M. J. Berg, N. R. Subedi, P. A. Anderson, *Opt. Lett.* **42**, 1011-1014 (2017).
9. M. J. Berg, G. Videen, *J. Quant. Spectrosc. Radiat. Transfer* **112**, 1776-1783 (2011).
10. J. P. Fugal, R. A. Shaw, E. W. Saw, A. V. Sergeev, *Appl. Opt.* **43**, 5987-5995 (2004).
11. A. Brodoline, N. Rawat, D. Alexandre, N. Cubedo, M. Gross, *Opt. Lett.* **44**, 2827-2830 (2019).
12. M. Brunel, B. Delestre, M. Talbi, *Rev. Sci. Instrum.* **90**, 053109 (2019).
13. O. Kemppinen, Y. Heinson, M. J. Berg, *Appl. Opt.* **56**, F53-F60 (2017).
14. S. Holler, M. J. Berg, O. Kemppinen, Y. W. Heinson, *Proc. SPIE* **10669**, Computational Imaging III, 106690B (2018).

References

- [1] P. Kulkarni, K. Willeke (eds.), *Aerosol Measurement: Principles, Techniques, and Applications* (Wiley, New Jersey, 2011), p. 752.
- [2] F. Joachim (ed.) *Electron Tomography: Methods for Three-Dimensional Visualization of Structures in the Cell*, 2nd ed., (Springer, New York, 2006).
- [3] A. J. Koster, U. Ziese, A. J. Verkleij, A. H. Janssen, K. P. de Jong, "Three-dimensional transmission electron microscopy: A novel imaging and characterization technique with nanometer scale resolution for material science," *J. Chem. Phys. B* 104, p. 9368-9370 (2000).
- [4] Y.-L. Pan, C. Wang, S. C. Hill, M. Coleman, L. A. Beresnev, J. L. Santarpia, "Trapping of individual airborne absorbing particles using a counterflow nozzle and photophoretic trap for continuous sampling and analysis," *Appl. Phys. Lett* 104, 113507 (2014).
- [5] N. D. Lho, et al., "Fractal morphology, imaging and mass spectrometry of single aerosol particles in flight," *Nature* 486, p. 513 (2012).
- [6] M. J. Berg, Y. W. Heinsohn, O. Kemppinen, S. Holler, "Solving the inverse problem for coarse-mode aerosol particle morphology with digital holography," *Sci. Rep.* 7:9400 (2017).
- [7] T. Kreis, *Handbook of Holographic Interferometry: Optical and Digital Methods* (Wiley, 2005), p.96.
- [8] M. J. Berg, N. R. Subedi, P. A. Anderson, "Measuring extinction with digital holography: Nonspherical particles and experimental validation," *Opt. Lett.* 42(5), p. 1011-1014 (2017).
- [9] M. J. Berg, G. Videen, "Digital holographic imaging of aerosol particles in flight," *J. Quant. Spectrosc. Radiat. Transfer* 112, p. 1776-1783 (2011).
- [10] J. P. Fugal, R. A. Shaw, E. W. Saw, A. V. Sergeyev, "Airborne digital holographic system for cloud particle measurements," *Appl. Opt.* 43(32), p. 5987-5995 (2004).
- [11] A. Brodoline, N. Rawat, D. Alexandre, N. Cubedo, M. Gross, "4D compressive sensing holographic imaging of small moving objects," *Opt. Lett.* 44, p. 2827-2830 (2019).
- [12] M. Brunel, B. Delestre, M. Talbi, "3D-reconstructions for the estimation of ice particle's volume using a two-views interferometric out-of-focus imaging set-up," *Rev. Sci. Instrum.* 90, 053109 (2019).
- [13] O. Kemppinen, Y. Heinsohn, M. J. Berg, "Quasi three-dimensional particle imaging with digital holography," *Appl. Opt.* 56(13), p. F53-F60 (2017).
- [14] S. Holler, M. J. Berg, O. Kemppinen, Y. W. Heinsohn, "Two-dimensional scattering and digital holography from isolated aerosol particles," *Proc. SPIE* 10669, *Computational Imaging III*, 106690B (2018).